Shell structure beyond the proton drip line studied via proton emission from deformed ^{141}Ho

M. Karny [a,b,1], K.P. Rykaczewski [c], R.K. Grzywacz [d,c], J.C. Batchelder [e], C.R. Bingham [d,c], C. Goodin [f], C.J. Gross [c], J.H. Hamilton [f], A. Korgul [a,b,d,f], W. Królas [b,f,g], S.N. Liddick [d,e], K. Li [f], K.H. Maier [c,b], C. Mazzocchi [d,h], A. Piechaczek [i], K. Rykaczewski [j], D. Schapira [c], D. Simpson [d], M.N. Tantawy [d], J.A. Winger [k], C.H. Yu [c], E.F. Zganjar [i], N. Nikolov [d], J. Dobaczewski [ℓ,m], A.T. Kruppa [n,b], W. Nazarewicz [d,c,ℓ], M.V. Stoitsov [d,c,o]

[a] *Institute of Experimental Physics, Warsaw University, Warsaw, PL 00681, Poland*

[b] *Joint Institute for Heavy Ion Research, Oak Ridge National Laboratory, Oak Ridge, TN 37831, USA*

[c] *Physics Division, Oak Ridge National Laboratory, Oak Ridge, TN 37831, USA*

[d] *Department of Physics and Astronomy, University of Tennessee, Knoxville, TN 37996, USA*

[e] *UNIRIB/Oak Ridge Associated Universities, Oak Ridge, TN 37831, USA*

[f] *Department of Physics, Vanderbilt University, Nashville, TN 37235, USA*

[g] *Institute of Nuclear Physics, Krakow, PL 31342, Poland*

[h] *IFGA, University of Milan and INFN, Milano, I-20133, Italy*

[i] *Department of Physics, Louisiana State University, Baton Rouge, LA 70803, USA*

[j] *Woodruff School of Mechanical Engineering, Georgia Inst. of Technology, GA 30332, USA*

[k] *Department of Physics, Mississippi State University, Mississippi State, MS 39762, USA*

[ℓ] *Institute of Theoretical Physics, Warsaw University, Warsaw, PL 00681, Poland*

[m] *Department of Physics, University of Jyväskylä, FI-40014, Finland*

[n] *Institute of Nuclear Research, Bem tér 18/c, 4026 Debrecen, Hungary*

[o] *Institute of Nuclear Research and Nuclear Energy, Bulgarian Academy of Sciences, Sofia, Bulgaria*

Article published in Elsevier Preprint (2008) 1–14

Abstract

Fine structure in proton emission from the $7/2^-[523]$ ground state and from the $1/2^+[411]$ isomer in deformed nucleus ^{141}Ho was studied by means of fusion-evaporation reactions and digital signal processing. Proton transitions to the first excited 2^+ state in ^{140}Dy, with the branching ratio of $I_p^{gs}(2^+)$=0.9±0.2% and $I_p^m(2^+)$=1.7±0.5%, were observed. The data are analyzed within the non-adiabatic weak coupling model assuming a large quadrupole deformation of the daughter nucleus ^{140}Dy as predicted by the self-consistent theory. Implications of this result on coexistence effects around N=74 are discussed. Significant modifications of the proton shell structure when going from the valley of beta stability to the proton drip line are discussed in terms of self-consistent theory involving the two-body tensor interaction.

Key words: proton radioactivity, proton shell structure, two-body tensor interactions
PACS numbers: 23.50.+z,21.10.Pc,24.10.Eq,27.60.+j

[1] Corresponding author: Institute of Experimental Physics, Warsaw University, PL-00681 Warsaw, Hoża 69, Poland; e-mail: karny@mimuw.edu.pl

1 Introduction

New experimental advances along the isospin axis require safe and reliable theoretical predictions of nuclear properties throughout the whole nuclear chart. In this context, of particular importance are experimental data for extremely proton-rich and neutron-rich nuclei in which poorly known components of the effective interaction, in particular in the spin-isospin channel, are amplified. The isospin dependence of the effective interaction and the presence of states that are unbound to particle-emission may have significant impact on spectroscopic properties of nuclei, e.g., variations in the single-particle (s.p.) shell structure [1].

Theoretical predictions and experimental discoveries in the last decade indicate that nucleonic shell structure is being recognized now as a more local concept [2–4]. In this context, a lot of attention has been given to neutron-rich nuclei where spectacular changes in the neutron shell structure have been seen, including the disappearance and emergence of magic gaps [5]. So far, there have been no strong indications of appreciable variations of the proton shell structure in proton-rich nuclei. The usual explanation is given in terms of the confining effect of the Coulomb barrier that (i) leads to spatial localization of narrow resonances above the proton emission threshold, and (ii) effectively shifts the non-resonant proton continuum up in energy. While many-body correlations in proton-rich systems are not going to be very different compared to stable nuclei, and the threshold effects are much less significant than on the neutron-rich side, one can certainly expect changes in the effective interaction when moving from the stability valley towards the proton drip line. To put things in perspective, the stable Ho isotope, $^{165}_{67}\mathrm{Ho}_{98}$ (T=31/2), contains 24 more neutrons as compared to the proton emitter $^{141}_{67}\mathrm{Ho}_{74}$ (T=7/2) discussed in this work. The corresponding change in the neutron shell structure implies appreciable variation in spin saturation, and this is expected to impact the tensor components of the interaction; hence spin-orbit fields [6–8].

Proton emitters are spectacular examples of open quantum systems and a wonderful playground to study coupling between bound and unbound nuclear states. Proton emitters also provide a wealth of spectroscopic information on proton and neutron shell structure in proton-rich nuclei. Measured proton energies, lifetimes, and proton branching ratios (fine structure) allow us to deduce the angular momentum of the emitted proton and to characterize its wave function inside the nucleus [9–12]. This, together with properties of collective states in neighboring nuclei, enables theory to fine-tune nuclear structure models.

This paper presents the first observation of fine structure in proton emission from two states in an odd-Z, even-N nucleus: the $7/2^-[523]$ ground-state and

$1/2^+[411]$ isomeric state in deformed ^{141}Ho. The measured decay properties are used to extract information on the wave functions of these unbound deformed Nilsson levels and on the proton mean field in this region.

The discovery of the proton-emitting ground state of ^{141}Ho ($T_{1/2}$=4.2(4) ms, E_p=1169(8) keV) [13] was followed by the observation of proton emission from a short-lived isomeric state ($T_{1/2}$=8(3) μs, E_p=1230(20) keV) at about 60 keV excitation energy [14]. The deformed Nilsson orbitals $7/2^-[523]$ and $1/2^+[411]$ were assigned to ^{141gs}Ho [13] and ^{141m}Ho [14], respectively. In a subsequent experiment [15], rotational bands built upon these deformed bandheads were identified. The experimental upper limit for the fine structure branching ratio $I(2_1^+)$ was quoted as 1% for both ground- and isomeric state assuming the energy of the rotational 2_1^+ state in ^{140}Dy to be $\leq$250 keV [15]. The 2_1^+ energy was later measured in Refs. [16,17] to be 202.2(1) keV suggesting a quadrupole deformation $\beta_2 \approx 0.23$-0.24 [18], and thus making ^{141}Ho, together with ^{131}Eu [19], a paradigm for a proton emission from a deformed nucleus.

2 Experiment

The ions of ^{141gs}Ho and ^{141m}Ho ions were produced at ORNL's HRIBF using fusion-evaporation reactions with a 20-35 particle nA ^{54}Fe beam impinging on a ^{92}Mo target. Beam energies of 300 MeV and 290 MeV were optimized for target thicknesses of 1.0 and 0.6 mg/cm^2, respectively. Reaction products were separated according to their mass-to-charge ratio, A/Q=141/25 and 141/26 by the Recoil Mass Spectrometer (RMS) [20]. RMS-selected recoils were implanted into a 65-microns thick Double-sided Silicon Strip Detector (DSSD, FWHM=18-25 keV for E_p=1.17 MeV) after passing trough a thin-foil, position-sensitive Micro Channel Plate (MCP) detector and being slowed down to about 60-70 MeV by a degrader foil. The flight time through the separator was 2.2 μs. The production cross sections were evaluated to be 1.4 μb at 300 MeV and 240 nb at 290 MeV for $^{141g.s.}$Ho and ^{141m}Ho, respectively, at the RMS transmission of 5%. In the first 90-hour experiment on $^{141g.s.}$Ho, the DSSD was backed with a 0.5-mm thick Si detector (FWHM=75 keV for E_α = 5.5 MeV). The signals from all detectors were read by the Digital Gamma Finder (DGF) modules [21] and analyzed on-board. The ^{141gs}Ho proton transition of 1169(8) keV [13] was used to establish the offset-free energy calibration of proton induced signals analyzed in the digital detection system [21]. The energy spectra of emitted protons were obtained using time and pixel correlations with implanted ions, requesting an energy difference below $\pm$ 4% for the coincidence signals recorded in the front and back DSSD strips [22], and requiring an anticoincidence condition with the Si detector behind the DSSD. For the ^{141m}Ho measurement (85 hours with a steady 35 particle nA ^{54}Fe beam), four 0.7-mm thick Si detectors forming sides of a box upstream

of the DSSD (Si-box) detecting the DSSD-escaping protons were added, and a 4-mm thick Si(Li) detector replaced the 0.5-mm Si counter [23]. The signals counted by the Si-box detectors (FWHM=60 keV for E_α=5.5 MeV) and Si(Li) detector (FWHM=120 keV for E_α=5.5 MeV) were used to veto the DSSD-recorded energy spectra and allowed us to reduce substantially the background below the main ^{141m}Ho proton peak, compare [24]. Due to the short half-life of ^{141m}Ho, the DGF modules serving the DSSD were programmed to trigger only for events where the recoil implantation signal was followed by the decay within the 0.5-40 μs time range ("proton-catcher" mode [25]). The waveforms (traces) containing both recoil and decay signals were stored for further analysis. For the sake of analysis of ^{141m}Ho data, a database of normalized single pulse reference traces was constructed. A full range trace fit, with two reference traces (for recoil and decay) and a constant baseline, was performed for each event. Scaling factors for both traces are free parameters of the fit and are proportional to the energy deposited by the heavy ion or proton in the DSSD. The offset-free energy calibration was performed using the Ep=959.7(28) keV protons [26] from ^{113}Cs decay ($T_{1/2}$=18.3(3) μs [27]) and verified using the main 1235(9) keV proton transition from ^{141m}Ho [15], see [24] for more details.

Figure 1 shows the energy spectrum of $^{141g.s.}$Ho decay signals between 1 ms and 16 ms after recoil implantation. Apart from the main peak and the proton escape events, a peak at the energy of 0.97 MeV was detected. The energy difference of 201(6) keV between the main peak and the satellite one is consistent with the energy of the 2_1^+ state in ^{140}Dy. The peak areas of 57(12) and 6360(80) counts in the satellite and main peak, respectively, yield the branching ratio $I_p^{gs}(2_1^+)$= 0.9(2)% for proton emission from $^{141g.s.}$Ho. One-component exponential fit to the decay pattern of the main peak gives a more precise half-life value of 4.1(1) ms for $^{141g.s.}$Ho. The energy spectrum of ^{141m}Ho decay events within 40 μs after ion implantation is presented in Fig. 2 (panel *a*). Panel *b* shows the decay pattern of the main peak together with the exponential fit yielding value of $T_{1/2}$=7.4(3) μs for ^{141m}Ho. The time distribution of satellite peak events is consistent with the half-life of 7.4 μs (panel *c*). The proton energy of 1.03(1) MeV agrees very well with the energy expected for the decay to the 2^+ excited state. On the basis of the observed half-life and energy, we assign the satellite peak to the proton transition from the ^{141m}Ho state to the first 2^+ excited state in ^{140}Dy. With 13 counts above the background of 4 counts for the satellite peak and 770(30) counts in the main peak the branching ratio for this transition was calculated to be $I_p(2^+) = 1.7(5)\%$.

3 Discussion

Decay properties of ^{141}Ho have been discussed in a number of theoretical approaches, differing in degree of sophistication [11,28–30]. Up to now, none of the theoretical approaches employed was able to explain *all* measured properties related to the structure and decay of ^{141}Ho and ^{141m}Ho, including lifetimes, branching ratios, and ordering of single-particle levels. This should not come as a surprise as decay properties of ^{141}Ho depend crucially on small components in the wave function that sensitively depend on the choice and magnitude of couplings considered. Namely, the lifetime of ^{141}Ho is governed by a small $\pi f_{7/2}\otimes 0^+$ component of the g.s. wave function of predominantly $h_{11/2}$ character. The increase in the $\pi f_{7/2}$ amplitude is immediately reflected by a faster proton emission. On the other hand, the decay of ^{141m}Ho to ^{140gs}Dy solely depends on a $\pi s_{1/2}\otimes 0^+$ component, while the transition to the 2_1^+ state (hence the branching ratio $I_p^m(2_1^+)$) depends on $\pi d_{3/2}\otimes 2_1^+$ and $\pi d_{5/2}\otimes 2_1^+$ partial widths (the $s_{1/2}$ wave is excluded by virtue of angular momentum conservation).

Proton emission calculations have been carried out within the non-adiabatic weak coupling model [31,32] in the recent variant based on the combination of the R-matrix theory and the oscillator expansion technique [11] that allows for a substantial increase of the number of coupled channels. We employed the same successful Chepurnov parameterization [33] of the Woods-Saxon (WS) optical potential as earlier in Ref. [32]. Compared to our earlier studies, we now consider the full deformed spin-orbit (s.o.) potential. (See Ref. [34] for the definition of the average deformed Hamiltonian.) The inclusion of deformation in the s.o. potential improves the description of the deformed $[411]3/2^+$ proton-emitting ^{131gs}Eu measured to have $T_{1/2}^p$=26.6(4) ms and $I_p^{gs}(2_1^+)$=24(5)% [19]. Assuming a spherical s.o. potential, one obtains $T_{1/2}$=34 ms and $I_p^{gs}(2_1^+)$=39% [32], while our improved calculations give $T_{1/2}$=18 ms and $I_p^{gs}(2_1^+)$=20% taking the BCS spectroscopic factor u^2=0.67.

Many structural properties of ^{141}Ho, including its spectrum and decay, depend on its shape deformation. While there is a consensus regarding the large elongation of this system, there is a considerable uncertainty regarding the actual value of quadrupole deformation β_2 of ^{141}Ho and its core ^{140}Dy. Figure 3 shows predicted values of $|\beta_2|$ for even-even Dy isotopes with $74\leq N\leq 102$ obtained in several theoretical models: Hartree-Fock-Bogoliubov (HFB) mass models of Refs. [35,36] with SLy4 [37], SkM* [38], and SkP [39] density functionals, the recent HFB14 mass model [40], and the Finite-Range Droplet Model (FRDM) [41]). For nuclei with $N>84$, experimental information on β_2 exists from $B(E2)\uparrow$ rates [18]; these values agree well with the global expression of Ref. [18], $\beta_2 = (466 \pm 41)E_{2^+}^{-1/2}/A$, representing systematic trends. For nuclei close to the stability line, theory does fairly well, with FRDM slightly underestimating experiment and HFB14 being on the high side. The situa-

tion becomes less clear for neutron-deficient nuclei with N<82. For N=74, all HFB models predict a strongly deformed prolate shape with β_2 ranging from 0.34 (SkP, SkM*) to 0.41 (HFB14). The FRDM value is again reduced as compared to HFB models, β_2=0.27, while the global fit yields $\beta_2\approx$0.23. The difference between the phenomenological expression and HFB calculations is rather surprising, considering the excellent agreement for heavier nuclei. In order to explain this puzzle, we first note that theory predicts a coexistence between prolate and oblate shapes in this region. The inset in Fig. 3 shows the oblate-prolate energy difference calculated in the SLy4+HFB model for even-even Sm, Gd, and Dy isotopes with $72\leq N\leq 80$. While N=72 and 74 isotopes are predicted to be prolate, a transition to an oblate configuration with $\beta_2\approx$–0.2 is expected at N=76. A similar result has been obtained in SkM*, SkP, and HFB11 models, as well as in FRDM and NL-SH models [42] where, however, the transition to oblate shapes occurs at N=78.

Coexistence between low-lying well-deformed prolate and less-deformed oblate configurations may be the reason for an unexpectedly large energy of the 2_1^+ state in ^{140}Dy and a pronounced steady increase in the moment of inertia of this nucleus up to $J^\pi=8^+$. Interestingly, a low-lying, even-spin, positive-parity excited band has been found in the lighter N=74 isotones of ^{136}Sm [43] and ^{138}Gd [44]. While this structure has been interpreted as a γ band, its reduced alignment and irregular behavior at low spins are not inconsistent with a coexisting configuration. The influence of triaxiality on $^{141g.s.}$Ho decay was studied in Refs. [28,11], and it was concluded that coupling to γ-vibrational states was not able to explain the experimental data.

In view of the above discussion, we adopted the HFB deformation β_2=0.35 and β_4=–0.05 for the coupled channel calculations. At this deformation, the [523]7/2$^-$ and [411]1/2$^+$ levels are nearly degenerate and appear at the Fermi level of Z=67. (A similarly large prolate deformation has been predicted in Ref. [45] based on the relativistic mean field theory.) With this prolate shape, taking the BCS values u^2([523]7/2$^-$)=0.84 and u^2([411]1/2$^+$)=0.81, our calculations give $T_{1/2}$=7.8 ms ($I(2_1^+)$=1.3%) and $T_{1/2}$=7.6 μs ($I(2_1^+)$=1%) for ^{141}Ho and ^{141m}Ho, respectively. The resulting g.s. wave function of ^{141}Ho g.s. is dominated by the $h_{11/2}$ component (78.2%); the total $f_{7/2}$ amplitude is 12.6%. This can be compared to 81% of $h_{11/2}$ and 11.5% of $f_{7/2}$ obtained at β_2=0.29 (and spherical s.o. potential) in [32]. The isomeric state ^{141m}Ho is predicted to be strongly mixed, with 6.7% of $s_{1/2}$ component. This can be compared to 11% of $s_{1/2}$ parentage in the previous version of our model.

While the reproduction of the data is quite fair, further refinements of the model are possible. They include: (i) inclusion of coupling with coexisting oblate (or triaxial) configuration in ^{140}Dy along the lines of Ref. [46]; (ii) inclusion of pairing interaction in the weak coupling approach (see Refs. [47,30] for treatment of pairing within the strong coupling scheme); and (iii) consid-

ering a more realistic optical model potential. The latter point is particularly important as the relative positions of s.p. levels can strongly impact amplitudes of small components of the wave function of the parent nucleus that govern proton emission.

Microscopically, significant variations of s.p. states with shell filling can be caused by the two-body tensor force that is sensitive to the effect of spin saturation. On a one-body level, variation of the phenomenological s.o. potential due to the tensor force was studied in the 1980s by either considering an average tensor contribution to the s.o. term [48] or by phenomenologically changing the s.o. strength with shell filling [49]. It is only very recently, stimulated by the new data on neutron-rich nuclei, that the self-consistent treatment of the effective tensor interactions has been reintroduced [6–8].

In order to examine the effect of the two-body tensor force on s.p. states of rare earth nuclei, we carried out spherical self-consistent HFB calculations with the SkO functional [50] with and without the tensor term [51]. The relative energies of $2f_{7/2}$ and $1h_{11/2}$ proton orbitals (determining the ^{141}Ho g.s. decay), and $2d_{3/2}$ and $3s_{1/2}$ (determining the ^{141m}Ho decay) are displayed in Fig. 4 as a function of neutron number. In both cases, inclusion of the tensor term produces an appreciable contribution to the splitting between crucial spherical shells when moving away from the line of beta stability towards the proton drip line. Moreover, the self-consistent mechanism present in the HFB results produces enhanced variations as compared to the WS model. Namely, the $2d_{3/2}$-$3s_{1/2}$ splitting of WS energies changes only by 20 keV when going from ^{165}Ho to ^{141}Ho.

In summary, decay properties of $7/2^-$ and $1/2^+$ states in deformed ^{141}Ho have been reinvestigated yielding more accurate half-life values of 4.1(1) ms and 7.4(3)μs, respectively. For the first time in proton radioactivity studies, fine structure in proton emission from different levels in the parent nucleus was detected, with branching ratios of 0.9(2)% ($7/2^-$) and of 1.7(5)% ($1/2^+$). The structure of proton-emitting states was reanalyzed using an improved non-adiabatic approach. Good agreement with experimental data was obtained without changing any parameter values but taking the increased quadrupole deformation as predicted by the self-consistent theory. The large deformation of ^{140}Dy (also used in [29]) is consistent with the known proton shell structure around Z=67. The apparent deviation from systematic trends at N=74 might be caused by coexistence effects predicted in this region by several mean-field approaches. To clarify the puzzle of abnormally large 2_1^+ energy, lifetime measurements for the low-spin yrast states of ^{140}Dy and a search for an excited collective band in this nucleus are required.

Finally, using the self-consistent HFB theory, we investigated the neutron number dependence of single-proton states in the Ho isotopes. We found sig-

nificant variations of proton shell structure with neutron number. The changes are caused by both the self-consistency mechanism and the two-body tensor force that significantly impacts the s.p. splitting. This result indicates a direction for future theoretical refinements of our model.

Acknowledgment

ORNL is managed by UT-Battelle, LLC, for the U.S. Department of Energy under Contract DE-AC05-00OR22725. This work was also supported by the U.S. DOE through Contract Nos. DE-FG02-96ER40983, DE-FG02-96ER40963, DE-FC02-07ER41457, DE-FG02-96ER41006, DE-FG05-88ER40407, DE-FG02-96ER40978, and DE-AC05-76OR00033; by the National Nuclear Security Administration through DOE Research Grant DE-FG03-03NA00083; by the Polish Ministry of Science; by the Foundation for Polish Science (AK); by the Academy of Finland and University of Jyväskylä within the FIDIPRO program; and by Hungarian OTKA grant no. T46791.

References

[1] J. Dobaczewski, N. Michel, W. Nazarewicz, M. Płoszajczak, and J. Rotureau, Prog. Part. Nucl. Phys. **59**, 432 (2007).

[2] J. Dobaczewski and W. Nazarewicz, Phil. Trans. R. Soc. Lond. A **356**, 2007 (1998).

[3] R.F. Casten and B.M. Sherrill, Prog. Part. Nucl. Phys. **45**, S171 (2000).

[4] D.F. Geesaman *et al.*, Ann. Rev. Nucl. Part. Sci. **56**, 53 (2006).

[5] R.V.F. Janssens, Nature **435**, 89 (2005).

[6] J. Dobaczewski, Proc. of the *3rd ANL/MSU/INT/JINA RIA Theory Workshop*, Argonne, USA, April 4-7, 2006, nucl-th/0604043.

[7] T. Otsuka, T. Matsuo, and D. Abe, Phys. Rev. Lett. **97**, 162501 (2006).

[8] B.A. Brown *et al.*, Phys. Rev. C **74**, 061303(R) (2006).

[9] P.J. Woods and C.N. Davids, Ann. Rev. Nucl. Part. Sci. **47**, 541 (1997).

[10] A.A. Sonzogni, Nucl. Data Sheets **95**, 1 (2002).

[11] A.T. Kruppa, and W. Nazarewicz, Phys. Rev. C **69**, 054311 (2004).

[12] L.S. Ferreira, M.C. Lopes, and E. Maglione, Prog. Part. Nucl. Phys. **59**, 418 (2007).

[13] C.N. Davids *et al.*, Phys. Rev. Lett. **80**, 1849 (1998).

[14] K. Rykaczewski *et al.*, Phys. Rev. **C60**, 011301 (1999).

[15] D. Seweryniak *et al.*, Phys. Rev. Lett. **86**, 1458 (2001).

[16] W. Królas *et al.*, Phys. Rev. C **65**, 031303R (2002).

[17] D. Cullen *et al.*, Phys. Lett. B **529**, 42 (2002).

[18] S. Raman, C.W. Nestor, and P. Tikkanen, At. Data Nucl. Data Tables **78**, 1 (2001).

[19] A.A. Sonzogni *et al.*, Phys. Rev. Lett. **83**, 1116 (1999).

[20] C.J. Gross *et al.*, Nucl. Instr. and Meth. A **450**, 12 (2000).

[21] R. Grzywacz, Nucl. Instr. and Meth. B **204**, 649, (2003).

[22] K.P. Rykaczewski *et al.*, AIP Conf. Proc. **638**, 149 (2002).

[23] M.N. Tantawy *et al.*, Phys. Rev., C **73**, 024316 (2006).

[24] M. Karny *et al.*, AIP Conf. Proc. **961**, 22 (2007).

[25] M. Karny *et al.*, Phys. Rev. Lett., **90**, 012502, (2003).

[26] S. Hofmann, Radiochimica Acta **70/71**, 93, (1995).

[27] C. J. Gross *et al.*, AIP Conf. Proc. **455**, 444 (1998).

[28] C.N. Davids and H. Esbensen, Phys. Rev. C **69**, 034314 (2004).

[29] L.S. Ferreira and E. Maglione, J. Phys. G **31**, S1569 (2005).

[30] A. Volya and C. Davids, Eur. Phys. J. A **25**, s01, 161 (2005).

[31] A.T. Kruppa *et al.*, Phys. Rev. Lett. **84**, 4549 (2000).

[32] B. Barmore *et al.*, Phys. Rev. **C62** 054315 (2000).

[33] V.A. Chepurnov, Yad. Fiz. **6**, 955 (1967).

[34] S. Ćwiok *et al.*, Comput. Phys. Commun. **46**, 379 (1987).

[35] M.V. Stoitsov *et al.*, Phys. Rev. C **68**, 054312 (2003).

[36] J. Dobaczewski, M. Stoitsov, and W. Nazarewicz, AIP Conf. Proc. **726**, 51 (2004).

[37] E. Chabanat *et al.*, Nucl. Phys. A **635**, 231 (1998).

[38] J. Bartel *et al.*, Nucl. Phys. **A386**, 79 (1982).

[39] J. Dobaczewski, H. Flocard and J. Treiner, Nucl. Phys. **A422**, 103 (1984).

[40] S. Goriely, M. Samyn, and J.M. Pearson, Phys. Rev. C **75**, 064312 (2007).

[41] P. Möller *et al.*, Atom. Data and Nucl. Data Tables **59**, 185 (1995).

[42] G.A. Lalazissis, M.M. Sharma, and P. Ring, Nucl. Phys. A **597**, 35 (1996).

[43] E.S. Paul *et al.*, J. Phys. G **19**, 861 (1993).

[44] E.S. Paul *et al.*, J. Phys. G **20**, 751 (1994).

[45] L. Geng, H. Toki, and J. Meng, Prog. Theor. Phys. **112**, 603 (2004).

[46] J.D. Richards *et al.*, Phys. Rev. C **56**, 1389 (1997).

[47] G. Fiorin, E. Maglione, and L.S. Ferreira, Phys. Rev. C **67**, 054302 (2003).

[48] M. Płoszajczak and M.E. Faber, Z. Phys. A **299**, 119 (1981).

[49] J. Dudek, W. Nazarewicz, and T. Werner, Nucl. Phys. A **341**, 253 (1980).

[50] P.-G. Reinhard *et al.*, Phys. Rev. **C60**, 014316 (1999),

[51] M. Zalewski *et al.*, unpublished,

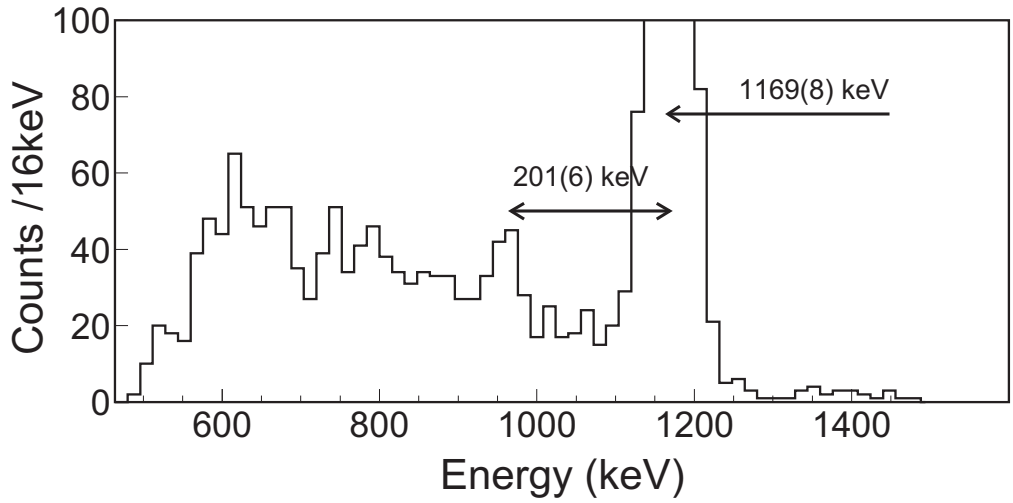

Fig. 1. The energies of decay signals within 1 to 16 ms after the implantation of ^{141}Ho ions. An energy difference of 201(6) keV was obtained for two observed proton peaks, the known transition at 1169(8) keV [13] and the peak at 0.97 MeV corresponding to a proton transition to the 202.1 keV 2^+ level in ^{140}Dy [16].

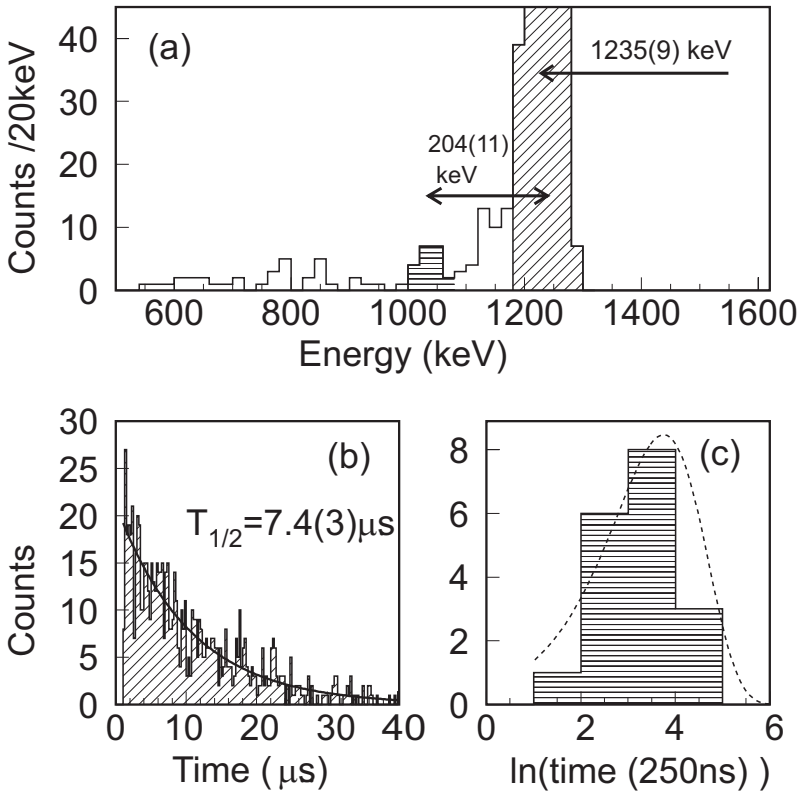

Fig. 2. (a:) energy spectrum of ^{141m}Ho decay signals between 0.5 and 40 μs after the recoil implantation. The energy difference of 204(11) keV between two observed peaks was determined using the calibration procedure based on the known 959.7(28) keV proton line from ^{113}Cs [26,27] and verified using known 1235(9) keV ^{141m}Ho proton peak [15]. Shaded areas correspond to the energy gates used in the lifetime analysis. The 1.17 MeV proton emission from 4.1 ms $^{141g.s.}$Ho resulted in about 20 counts present in the spectrum at the left side of the 1235 keV line. Panel b shows the decay pattern of the main peak together with the exponential fit yielding a more precise value of $T_{1/2}$=7.4(3) μs microseconds for ^{141m}Ho. (c:) decay pattern of the 1.03 MeV line (horizontally hashed) together with predicted shape for the $T_{1/2} = 7.4$ μs decay.

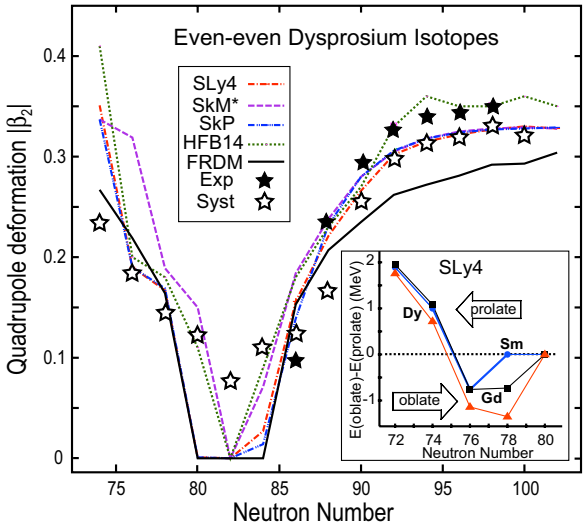

Fig. 3. Comparison between experimental ($\star$; from [18]) and calculated (SLy4, SkM*, and SkP HFB models [35,36]; HFB14 [40]; FRDM [41]) quadrupole deformations of even-even Dy isotopes with $74 \leq N \leq 102$. Results of the global best fit of Ref. [18] are also shown (open stars). The oblate-prolate energy difference calculated in the SLy4+HFB model for even-even Sm, Gd, and Dy isotopes around $N=76$ is shown in the inset.

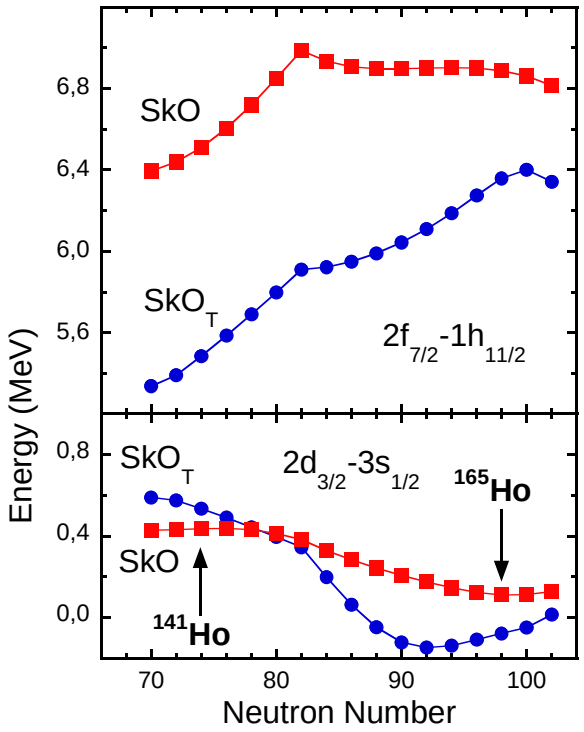

Fig. 4. The impact of tensor interaction on single-proton canonical states in the Holmium isotopes with $70 \leq N \leq 102$. Upper panel: energy difference between $2f_{7/2}$ and $1h_{11/2}$ levels. Lower panel: energy difference between $2d_{3/2}$ and $3s_{1/2}$ levels. Calculations were carried out within the spherical HFB approach without (SkO) and with (SkO$_T$) inclusion of the two-body tensor interaction [51].